1 Summary

This document describes the determination of the accuracy of the UVOT grism wavelength calibration based on the adjusted Zemax optical model.

2 Relevant Documents

- TBD

3 Scope

Description of the wavelength calibration method. The determination of the accuracy of the wavelength calibration of the UV Grism Nominal Mode.

4 Data used

Table 1 lists the calibration data used.

TABLE 1. UVOT observations of Wolf-Rayet stars used for the nominal UV grism calibration

ID	Object	OBSID	EXT	Grism image	Lenticular Filter Image	Date
1	WR52	56950007	1	gu231139384I	w1231394014I	080502
2	WR86	57000005	1	gu231383283I	w1231383514I	080502
3	WR52	56950007	2	gu231399443I	w1231399744I	080502
4	WR86	57000005	2	gu231388883I	w1231389214I	080502
5	WR1	37905003	1	gu238539623I	w1238540074I	080723
6	WR86	57011002	1	gu236456305I	w1236456305I	080629
7	WR86	57012002	1	gu236462064I	w1236462424I	080629
8	WR86	57013002	1	gu236543063I	w1236543424I	080629
9	WR86	57014002	1	gu236548824I	w1236549185I	080630
10	WR86	57018001	1	gu242197488I	w1242197979I	080904
11	WR86	57018002	1	gu242198243I	W1242198694I	080904
12	WR86	57015001	1	gu242208781I	W1242209111I	080904
13	WR86	57015002	1	gu242209403I	W1242209793I	080904
14	WR86	57016001	1	gu242214541I	W1242214932I	080904
15	WR86	57016002	1	gu242215284I	W1242215614I	080904
16	WR86	57017001	1	gu242220361I	W1242220692I	080904
17	WR86	57017002	1	gu242220983I	W1242221375I	080904
18	WR86	57019001	1	gu244152311I	W1244152640I	080926
19	WR86	57019002	1	gu244152983I	W1244153285I	080926
20	WR86	57020001	1	GU244158133I	W1244158463I	080926
21	WR86	57020002	1	GU244158743I	W1244159074I	080926
22	WR86	57021001	1	GU244163953I	W1244164284I	080926
23	WR86	57021002	1	GU244164564I	W1244164864I	080926

TABLE 1. UVOT observations of Wolf-Rayet stars used for the nominal UV grism calibration						
ID	**Object**	**OBSID**	**EXT**	**Grism image**	**Lenticular Filter Image**	**Date**
24	WR86	57022001	1	GU244169713I	W1244170043I	080927
25	WR86	57022002	1	GU244170324I	W1244170655I	080927
26	WR86	57023001	1	GU244175414I	W1244175745I	080927
27	WR86	57023002	1	GU244176024I	W1244176505I	080927
28	WR86	57024001	1	gu244238954I	w1244239285I	080927
29	WR86	57024002	1	gu244239564I	w1244239863I	080927
30	WR86	57025001	1	gu244244953I	w1244245283I	080927
31	WR86	57025002	1	gu244245563I	w1244245864I	080927
32	WR86	57026001	1	gu244250533I	w1244250864I	080927
33	WR86	57026002	1	gu244251144I	w1244251443I	080927

5 Introduction

The UVOT has two grisms mounted on each filterwheel, a *visible* and *uv* grism, and each grism has two standard modes of observation. The nominal mode is where the filterwheel aligns the axis of the grism with the optical axis in the same manner as the lenticular filters are used. In the so called “clocked” mode, the filterwheel is rotated less, thereby blocking part of the field of view. This reduces the number of stars in the field and allows the first orders to be less contaminated by zeroth orders.

The wavelength calibration is based on the UVOT *Zemax* optical model. Since the model does not include the fiber taper, correction factors were determined by comparing to observations of Wolf-Rayet stars, WR52 and WR86 which show an abundance of well-defined spectral lines down to the UV which are well matched with the spectral resolution. A comparison of the corrected *Zemax* model with ground calibration data shows that the model fits well.

The reference point for the wavelength scale on the image will be referred to as the “anchor point”.

First the methods used to perform the calibration are discussed, followed in section 7 by an assessment of how accurate the wavelength calibration is, by comparing spectral line wavelengths with known wavelengths.

The input angle of the source to the boresight along the DET image axes is used as a reference to look up the relevant parameters in a table. These are the wavelength anchor point at 2600 Å in the first order as well as all the dispersion coefficients and the location of the other orders. The first order wavelengths are determined (expressed as a set of polynomial coefficients) from the pixel coordinate along the rotated spectrum with reference to the anchor point. The wavelength coefficients of additional orders are

provided in a similar way. Currently, only the first order has been calibrated, and the second order dispersion information has been provided for development purposes.

6 Method used of determining the wavelength calibration

6.1 Use of the *Zemax* UVOT optical model

The *Swift* UVOT optics was designed using a *Zemax* optical model (e.g., http://www.zemax.com). The model includes telescope optics, and models for the lenticular filters and the grisms. It does not include the fiber taper optics nor the CCD, i.e., no correction for the distortion due to them, hence the pixel scale needs to be worked out.

Our approach has been to use the distortion determined for the lenticular filters, thereby assuming that the distortion seen in the lenticular filter images is mostly due to the fiber taper optics, and that the contribution to that distortion from the lenticular filters is relatively small. This has been mostly borne out by the calibration with only a small correction remaining to be made at the end.

The standard *Swift* UVOT processing corrects the RAW grism image using the distortion as determined from the lenticular filters, to produce the DET image (e.g., `sw00056950007ugu_dt.img`). The RAW and DET images use different coordinate systems. In the calibration file, the DET coordinates have been used after conversion to pixel coordinates with the centre of the image at (1100.5,1100.5), which are called DET-pixel coordinates for clarity.

6.2 Finding the input angle from the sky position

The source position on the sky needs to be translated into the angle of the input ray from the source with respect to the instrument boresight. The boresight is the direction on the sky for which the location of the source image on the detector will not change when the instrument is rotated around the boresight. For a lenticular filter the source image on the detector will be centered on one pixel location, the borepoint. For a grism image, a whole spectrum will fall on the detector. The spectrum for a source at the boresight will always fall on the same location of the image. As a reference point for the (first order) wavelength calibration, the 2600 Å point in first order has been chosen for the *uv* grisms, mainly because the optical model has used that wavelength as a reference also. As a result, the design of the telescope places the 2600 Å point in first order near the centre of the detector.

In order to simplify the lookup of parameters in the calibration file, the input angle has been provided on a rectangular grid in (X,Y) aligned with the detector image, and thus the DET coordinates. The grid thus neatly covers the detector image.

6.3 Determination of the boresight position for the grism image at 2600 Å in first order

Since the optical model is not complete, the model needs to be aligned with the observed boresight. This means that the boresight position needs to be determined at 2600 Å. This was done using WR stars which have very strong emission lines at, for example, 2398, 2405, 2530 Å. Five observations were taken attempting to position the source as closely to the boresight as possible. In all cases, the grism spectrum observation was directly followed by an observation in the *uvw1* filter, which can then be used to determine the offset of the boresight, since the boresight for *uvw1* is known.
The spectral lines in the image were identified and their position measured to determine the position of the 2600 Å point by interpolation. The boresight point in the image at 2600 Å in first order was found to be at [1005.5, 1079.7] (DET-pixel coordinates) with an uncertainty of 2 pixels in X and Y.

6.4 Model scale factor for the dispersion dimension

The *Zemax* model calculation provided for each input angle the position of the peak intensity at selected wavelengths in five orders, the zeroth order, and the first, second, third and minus first orders. For the spectra taken near the borepoint position, the predicted and observed wavelength as a function of pixel distance were compared. It was found that the model dispersion needed to be scaled by a factor 0.960 for a good fit. Comparison to the pre-launch ground calibration gave the same factor. The scale factor does not only provide a good match between model and observations of the wavelengths in the first order, but also works for the zeroth and second order in the ground calibration data for which this could be verified. In the observations we have unfortunately not been able to identify features to assign a wavelength in the zeroth or second order.

6.5 The anchor point position in the calibration image

For all calibration observations, the anchor point position (the 2600 Å, first order point in the image) was determined as outlined above. The unscaled model positions for the 2600 Å, first order anchor points were found to be close to the observed ones, but a small correction improved the accuracy in the dispersion direction, especially for points further out. The main factor in the correction is a scale factor of 0.9815, but it is offset from the borepoint position, centered around (1026.2,1142.5). The reason may lie in an overcorrection of the distortion which was based on the lenticular filter measurements. The lenticular filters are shaped to correct for some telescope optics, and have different centre. This empirical correction (not to be confused with the independent scale factor that applies to the dispersion only) was applied in the calculation of the calibration file.

6.6 Fitting to ground calibration data

Before launch, in November 2002, the complete UVOT instrument had a ground calibration at the NASA Goddard Space Flight Center. The calibration of the grism could only be done for one position, along the central axis which corresponds closely to the

boresight of the instrument. The light source used was a Pt/Cr/Ne Lamp, while several broadband filters could be inserted into the light path entering the telescope.

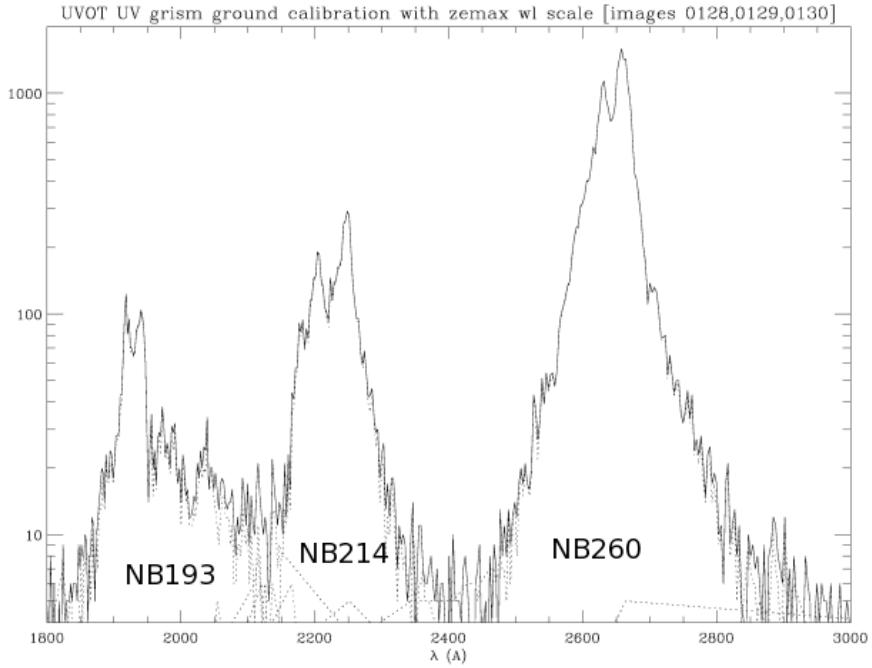

Figure 1. Combined in one figure are three observations with the measurements from the three broad-band filters along the dispersion direction in the first order. The observations were taken in sequence with the source on-axis. The dotted lines show the individual filter contributions. The strongest lines visible are at 1930, 2175, 2203, 2246, 2631, and 2660Å.

In order to fit the observations and the calibration, the observation was found to have a slightly different angle for the dispersion plane, at an angle of about 68.8^{o}, while the design was 65^{o}. The correction of 3.8 degrees was incorporated into the model calculations. The scale factor derived from the measured line positions is consistent with the factor 0.960 that we used in the calibration. The model also predicts quite well the zero and second order positions measured in the ground calibration.

The relative countrates of the main lines each broadband filter give an indication of the relative response in second to first order and zeroth to first order. We find that the ratio of total intensities in the second/first order are about 0.80 at 1930Å, 0.42 at 2220Å, and 0.22 at 2645Å. The response is also sensitive to the dispersion, so these ratios should be divided further by a factor 2. Note that the response ratio is not flat, and the errors are within 3%, so the second order response is different from the first order response.

The same can be done for the zeroth/first order ratio. The ratios for the same wavelengths as above are 0.08, 0.07, 0.44. The low ratio around 2100Å is also seen in the few spectra

with a uv-tail to the zeroth order, where the short end often is disconnected from the main (visibe part) of the zeroth order.

6.7 Fitting to Wolf-Rayet spectra across the detector

The spectra are not dispersed with the same angle across the detector. The Zemax model predicts the variation of the angle over the detector. The angle at the anchor point was used for extracting the spectra. The image was rotated around the anchor point by the angle (about 151.2 deg), and a strip containing the spectrum and background is extracted. The anchor point is generally not centered exactly on the spectrum, so a projection of the anchor point to the peak of the spectrum was made. Then the wavelength was computed using the interpolated model prediction.

The spectra show several well-defined carbon lines and some weak He lines at 1909, 2297, 2405, 2530, 2906, 3409, 4069, 4649, and 5803 Å. There are more lines, which are often blended. Second order lines were not readily found.

The well-identified lines in the spectrum are then used to determine the accuracy of the predicted wavelength. Initially this was done for the case of no empirical correction for the anchor point position, and the results were used to support the determination of the empirical correction independently, since the offset from the peak and offset from the wavelengths in the observations provide an independent (but rotated) measure of the anchor point error in X and Y. After application of the empirical correction, the remaining error in wavelengths was found to be 5 pixels (1σ) after removing some outliers which were attributed to spacecraft drift that occasionally happens during an observation. Support for that explanation is found in that the outliers occur all over the detector, and show no discernable pattern. Later observations for the clocked mode were done with lenticular filter observations both before and after the grism exposure, and they show that this indeed can happen.

In the next section results from the calibration file were directly compared to the observations and they give the same results.

7 Description of Analysis

The details of the determination of the grism wavelength calibration are described in section 6.

The spectrum in the image was extracted and spectral lines were identified. The locations of the lines on the image were then used to determine the location (X_{obs},Y_{obs}) of the anchor point on the image.

The input angle (X_{phi},Y_{phi}) of the input ray from the boresight were determined using the image in the lenticular filter. Since the source is very bright in the lenticular filter, the

procedure used was as follows: (1) the *uvw1* sky image was aspect corrected and checked; (2) the RA, DEC, and header information of the *uvw1* image was then used to determine the location of the source on the detector in DET(mm) coordinates, which was checked using DS9; (3) after conversion of the DET coordinate to pixels (using the conversion factor 0.009075 mm/pixel), the pixel difference in X and Y on the detector was determined from the offset of the known boresight of the lenticular filter; (4) the difference in pixels was used with the scale factor of 0.502"/pixel to determine the input angle.

The input angle was used to do a lookup of the parameters using bilinear interpolation in the calibration file prepared by us, to determine the predicted anchor position (X_{ank},Y_{ank}), the angle θ, which describes the angle of the first order on the detector image near the anchor point and the dispersion coefficients C_{1j} for the wavelength scale.

In Table 2 the measured and calculated anchor position, and input angle have been listed using the positions in the image. The measured positions on the image are related to the DET-pixel coordinates by adding (104,78) to the coordinates for $(X,Y)_{obs}$ and $(X,Y)_{ank}$ in Table 2.

Observations with ID 28 and 30 were too close to the edge of the detector to find an anchor point by simple bilinear interpolation. No extrapolation was attempted, although the original calibration did use these data.

Table 2. Observed and predicted anchor positions on the image and the input angle of the incoming ray.

ID	X_{obs}	Y_{obs}	X_{phi}	Y_{phi}	X_{ank}	Y_{ank}
1	905	995.1	0.00066	-0.00068	904.5	995.5
2	917.5	992.1	0.00250	-0.00176	916.2	988.7
3	916.9	991.3	0.00232	-0.00144	915.1	990.7
4	923.2	999	0.00306	-0.00051	919.7	996.7
5	877.4	1009	-0.00318	0.00142	880.1	1008.6
6	947.2	1021.2	0.00668	0.00264	942.5	1017.0
7	801.9	1073.9	-0.01642	0.01086	796.4	1067.8
8	895.9	1116.8	-0.00167	0.01752	889.3	1111.2
9	??	978.9	-0.00419	-0.00405	874.0	973.7
10	1046.5	767.9	0.02144	-0.03827	1038.4	756.0
11	1068	769.1	0.02609	-0.03729	1068.0	762.4
12	1135.3	1167	0.03484	0.02377	1121.0	1153.3
13	1130.1	1190.8	0.01959	0.02490	1134.6	1185.7
14	809.3	1155.4	-0.01708	0.02184	801.4	1151.6
15	724.3	1262.4	-0.02740	0.04051	737.1	1274.2
16	667.4	779.9	-0.05671	-0.04050	661.2	772.8
17	646	851.1	-0.03982	-0.02373	657.7	856.1

Table 2. Observed and predicted anchor positions on the image and the input angle of the incoming ray.

ID	X_{obs}	Y_{obs}	X_{phi}	Y_{phi}	X_{ank}	Y_{ank}
18	1162.1	685	0.02328	-0.05101	1162.0	700.0
19	1491.7	668.5	0.09335	-0.05127	1502.2	673.3
20	1102.3	1082.3	0.01582	0.01082	1110.9	1095.8
21	1403.5	1217.1	0.06141	0.02834	1402.7	1209.7
22	758.5	1598	-0.03820	0.09105	769.7	1599.6
23	1028.7	1652.4	0.00257	0.09773	1026.9	1645.9
24	540.4	1538.9	-0.07202	0.08193	558.1	1538.4
25	691.7	1499.9	-0.03133	0.07736	703.1	1487.4
26	237.3	1672.7	-0.10971	0.10977	219.4	1680.5
27	489.2	1786.6	-0.08311	0.11945	491.5	1772.2
28	62.1	1228	-0.15208	0.03472		
29	307.7	1349.6	-0.11069	0.05035	317.3	1335.1
30	86	703.3	-0.12996	-0.04338		
31	373.5	824.1	-0.09934	-0.03206	387.3	814.6
32	444.2	368.5	-0.09012	-0.09966	448.2	382.4
33	702.4	409.5	-0.04824	-0.09609	711.0	407.4

The angle 180-θ is used for extracting the spectrum and defining the direction on the detector for the dispersion.

The wavelengths can be found from the formula:

$\lambda = \Sigma_{j=0,n} C_{1j} p^n$

With λ the wavelength in Å and p the pixel-distance to the anchor point along the direction defined by the angle θ. Similarly, for the second order the coefficients are C_{2j}. The second order dispersion is referenced to the anchor in first order. The second order position and dispersion has been derived from the optical model as described in section 6, but has so far only been verified against ground calibrations at the boresight. The zero order, which also has only been verified with the ground calibration at the boresight position, is planned to be included in future releases.

Note that the dispersion is *not* defined by following the curvature of the spectrum, but by projection onto the line defined by the anchor point and 180-θ.

7.1 Accuracy of the anchor point

The anchor points derived from bilinear interpolation in the calibration file are compared to the observed positions (see Table 2) by rotating the difference in X and Y to compute

the pixel difference along the dispersion direction Δλ ((pixels; 1pixel = 3.1 Å). The histogram is shown in Fig. 2.

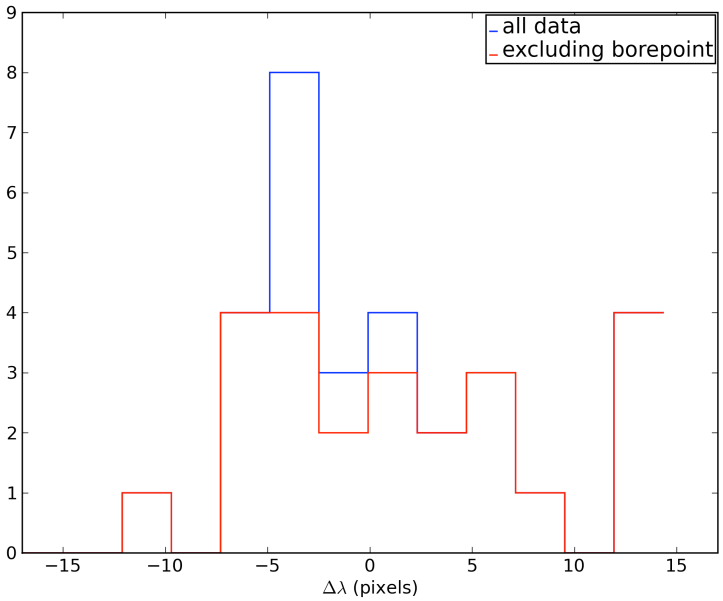

Figure 2: The comparison of the anchor position found from the source RA,DEC and the calibration file, to the one determined independently using the spectral line positions in the image.

The positions on the detector are shown in Fig. 3. As can be seen, the measurements are spread over the whole face of the detector, so the accuracy shown in Fig. 2, applies for the whole detector. Near the centre of the detector, it is slightly better. The 5 data points with a very high value for Δλ (see Table 2) are observations suspected to have drifted during the observation. These occur in no specific area of the detector which supports that notion. Ignoring these, the histogram, which compares the actual position from that determined using the source sky position with the calibration file, shows that the wavelength scale anchor point accuracy is about 5 pixels (RMS), or 15 Å. These results are virtually identical to the results obtained during the calibration discussed in section 6.

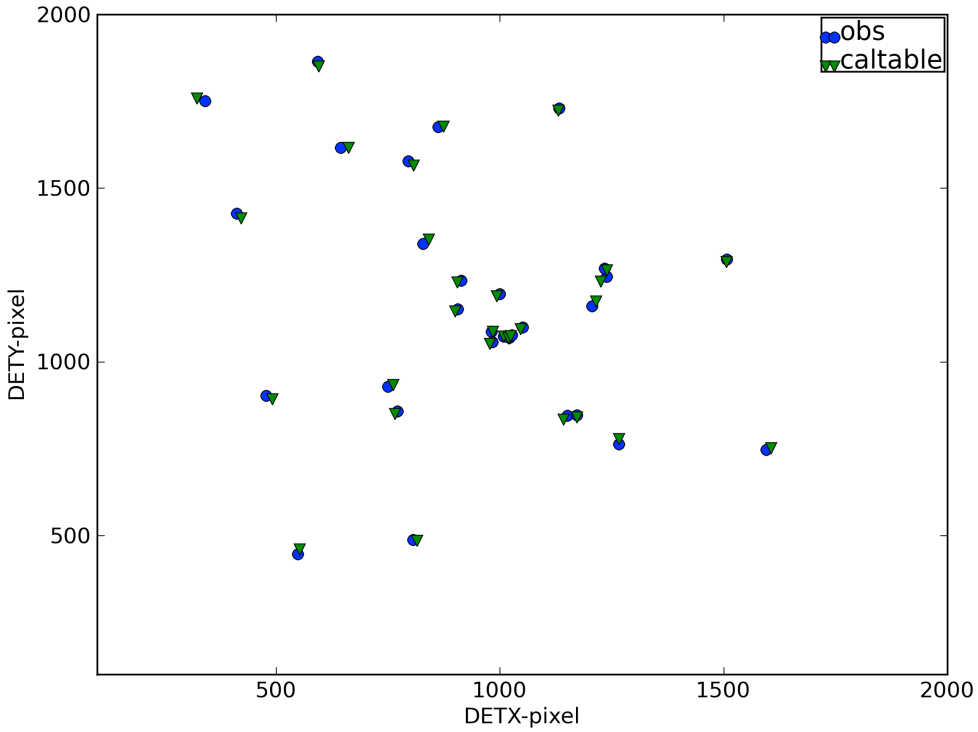

Figure 3. The observed anchor points are blue, and the ones derived using the calibration file are green triangles. The coordinate system is the DET coordinates converted from mm to pixels and the centre at [1100.5,1100.5].

7.2 Accuracy of the wavelengths using the calibration file

In section 6 the discussion of the calibration introduces two error sources for the wavelength accuracy. The first error is how accurately the anchor position of the wavelength scale can be determined from the sky position of a source, or equivalently, from the position in an image taken in a lenticular filter together with the grism in one observation sequence. The second source of error is how accurate the wavelength scale is over the whole range from 1750-6500 Å.

The accuracy of the determination of the anchor position using the calibration file has been discussed in section 7.1. We now consider the accuracy of the wavelength determination over the whole range, by comparing measured line positions in the extracted spectrum to their known positions. The coefficients of the dispersion polynomial from the calibration were interpolated using the input angle to derive the dispersion relation for each observation.

The accuracy of the calibration is shown in the figures below. Figures 4a,b use the calibration table, while figures 5a,b use the fit from the calibration itself which is the same to within 1 Å.

Any inaccuracies in the position of the anchor show up as a common shift of the observed differences in wavelength; inaccuracies in the form of the dispersion relation will show as a gradual difference of the observed points from the model points (+ signs) or the polynomial fit (the line) in the top panel. Inaccuracies in the measurements of the wavelengths will result in a spread in the lower panel.

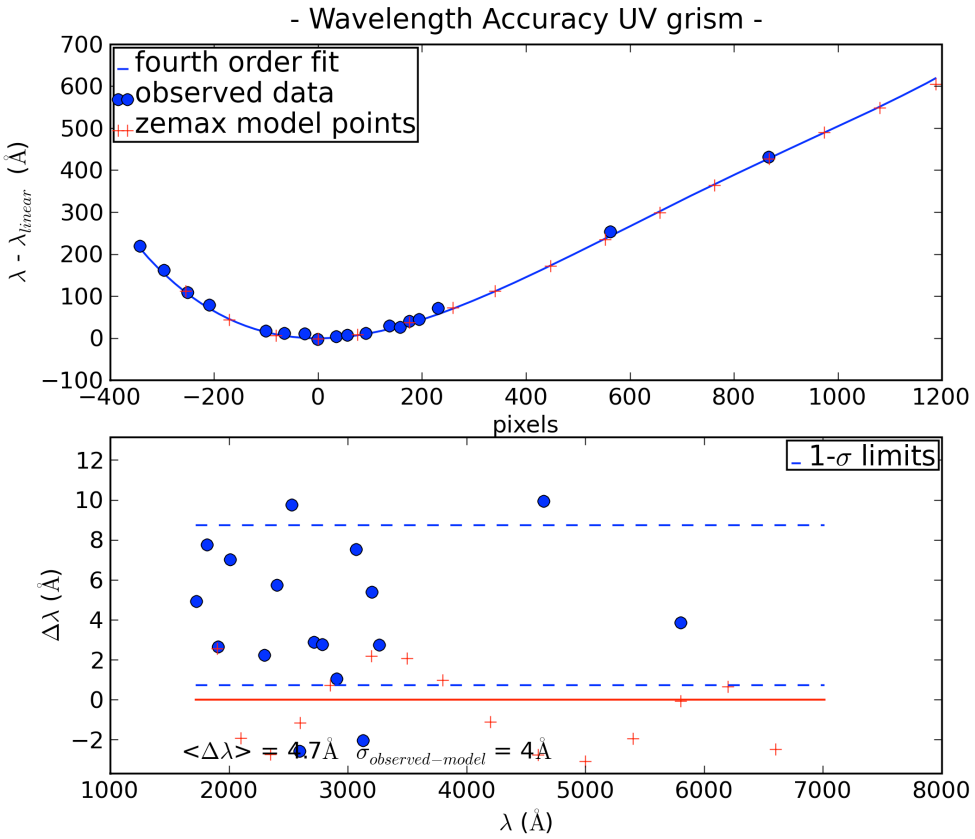

Figure 4a. This figure is for a spectrum (Table 1 ID=1) falling nearly on top of the boresight. The top panel shows as a function of pixel distance to the anchor at 2600 Å the residual wavelength difference after subtraction of the linear dispersion term which by definition gives zero at the anchor position. The crosses are the prediction of the Zemax optical model; the dots are measured from the image; and the blue line is the best fit through the model. The bottom panel compares the model with the observations with the model value set to zero.

It can be seen that the fit in Figure 4a is quite good, and the mean offset of the wavelength differences which is due to inaccuracies in the anchor position is here about 4 Å, which is slightly more than one pixel. The spread in the wavelength differences is consistent with the line widths in the spectrum.

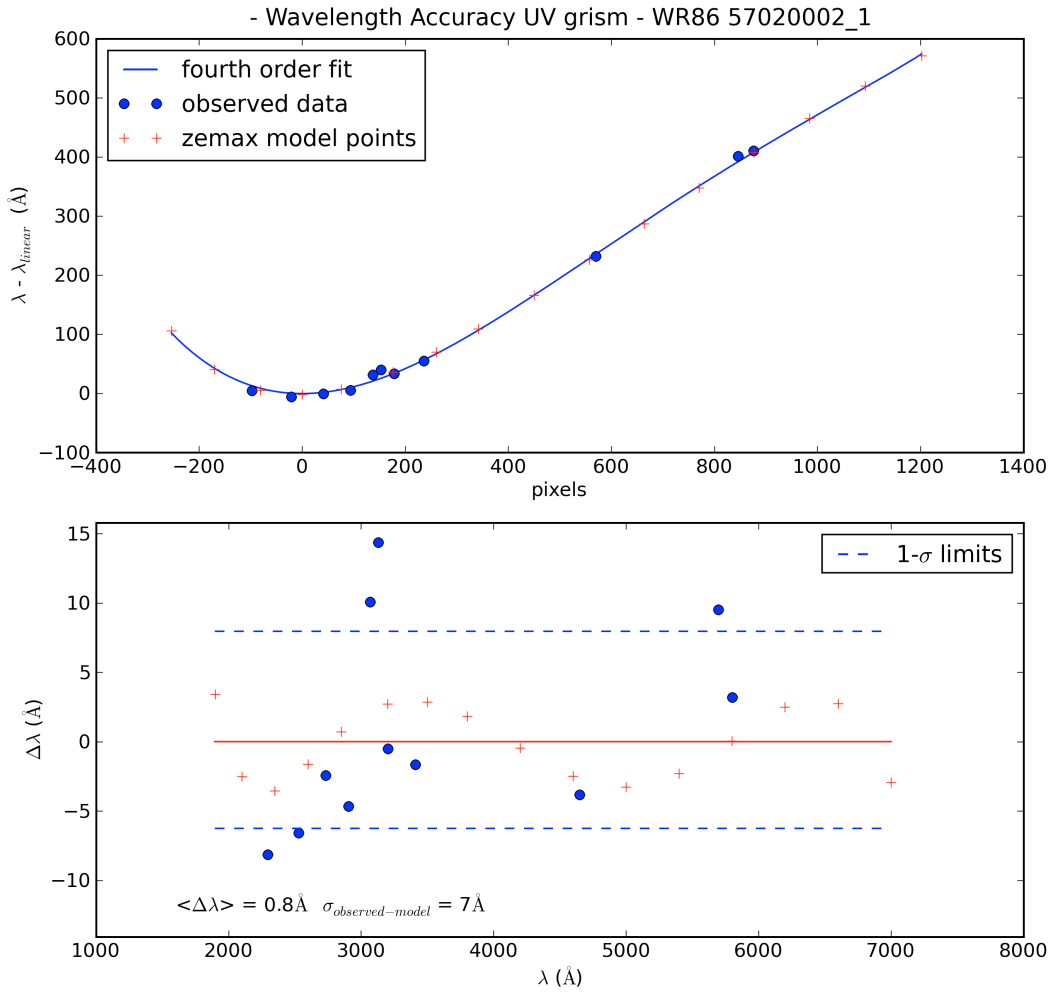

Figure 4b. Same as figure 4a but for (ID=21 in table 1).

Figures 4a is for a position near the boresight, and shows a typical picture seen in all the calibration observations. Figure 4b is several hundreds of pixels away from the boresight.

The following figures 5a,b, and c were not made using the calibration file, but by direct interpolation in the Zemax model which is not considered to affect the results. They were done for several points on the detector with anchors away from the boresight. The dispersion relations for those points are different from those at the boresight. Figure 5a

shows a slight trend in the disagreement between the observed and predicted wavelength. However, the difference is smaller than 10 Å. The largest difference in dispersion between model and observations occurs very close to the detector edge, and is still reasonably small. With that we mean that these inaccuracies are small compared to the uncertainty from the anchor position and relative to the resolution.

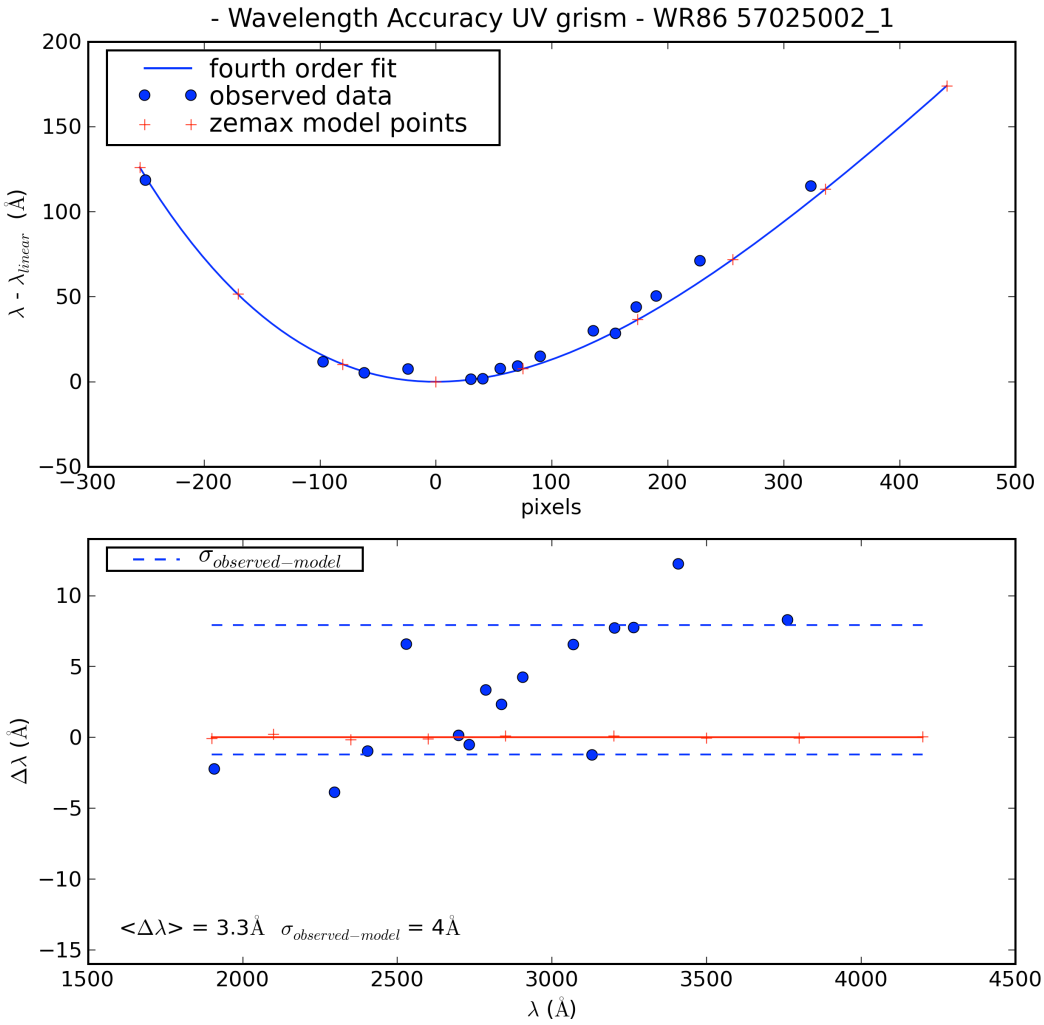

Figure 5a. Same as in Figure 4a, for a different position (ID=31 in table 1).

The accuracy found from these fits includes the uncertainty in anchor position, so a comparison to Figure 2 is useful. It was found to be consistent. Our tests show that the absolute wavelength accuracy is dominated by inaccuracies in the anchor point position and is about 15Å rms. The internal accuracy (i.e., neglecting the uncertainty of the anchor point) within the wavelength scale is better than 5 Å near the boresight, and around 12 Å near the edge of the detector. The accuracy knowledge has some limitations due to small number statistics in the number of calibration stars used.

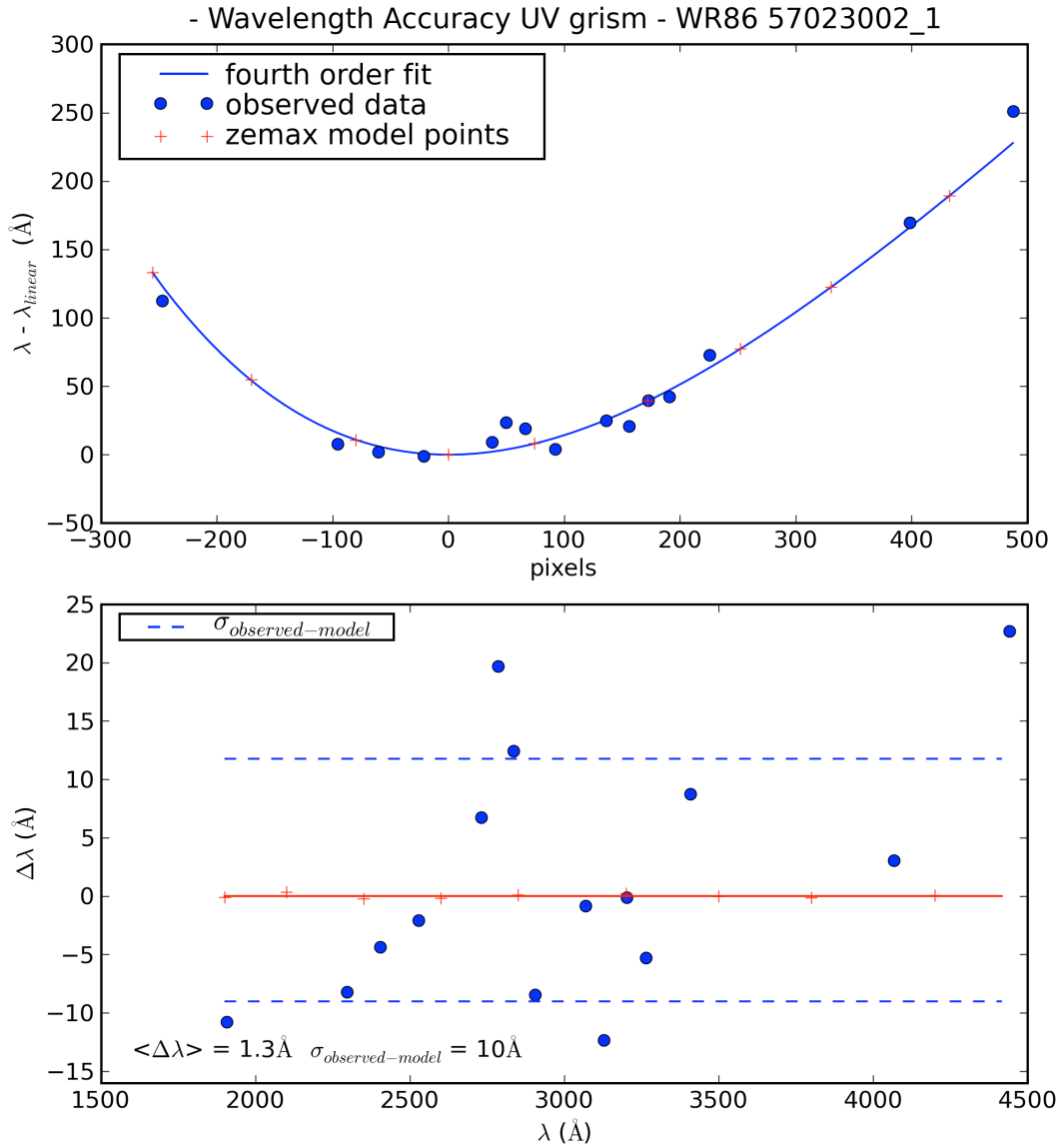

Figure 5b. Same as in Figure 4a, for a different position (ID=27 in table 1).

However, the overall consistency provided by the optical model gives a common benchmark against which all these observations have been tested, and to some extent provides an understanding of the variation over the detector of that uncertainty. We think that the current wavelength calibration is good enough to be used over the whole detector to yield wavelengths accurate within the stated uncertainties.

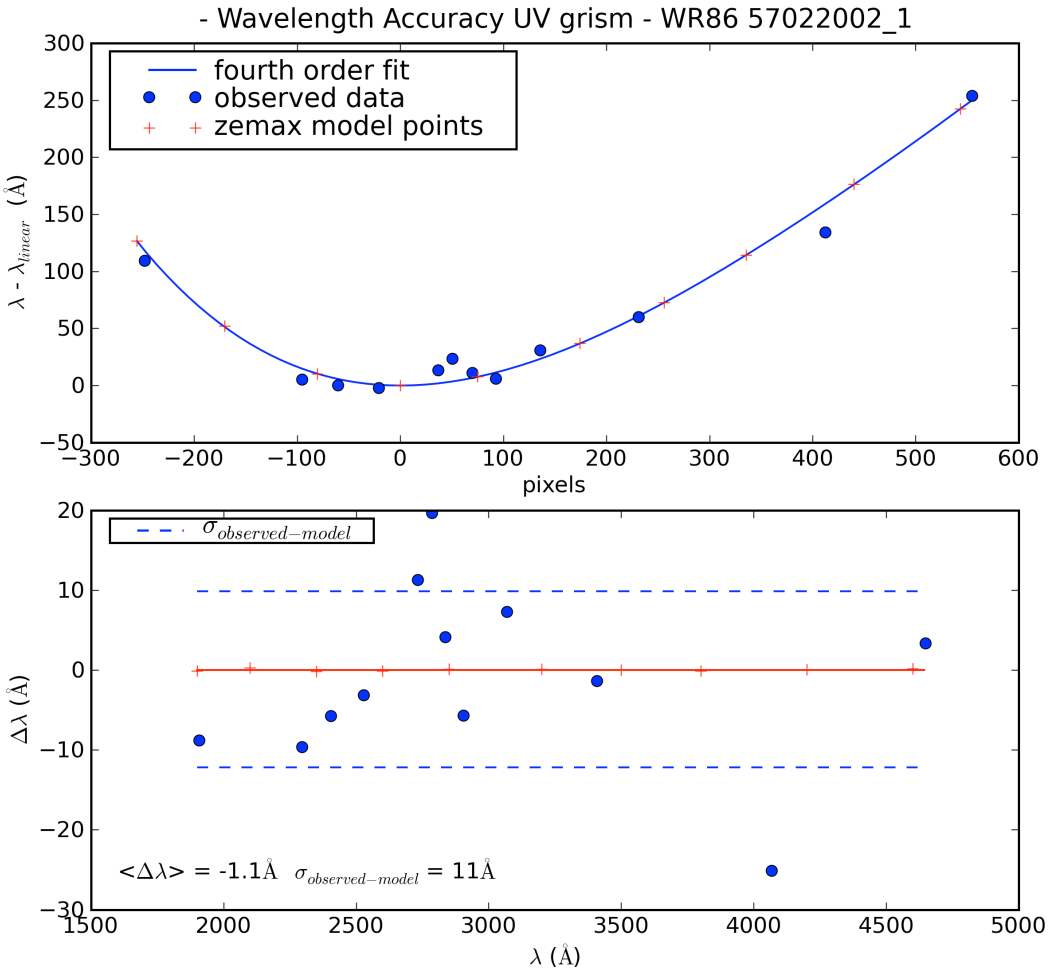

Figure 5c. Same as in Figure 3a, for a different position (ID=25 in table 1).

8 Summary

The wavelength accuracy using the anchor points and dispersion coefficients from the calibration file was found to be 15 Å (1σ) and is valid over the face of the detector.